

國立臺灣大學理學院地質科學所

碩士論文

Department of Geosciences

College of Science

National Taiwan University

Master Thesis



研究2006至2007年臺灣區域60個 $M_w > 3.3$ 的地震造成
的T波之傳播路徑、振幅大小和轉換效率

**T-waves Excited by 60 $M_w > 3.3$ Earthquakes in
Taiwan Region During 2006-2007: Implications of
Their Ray Paths, Amplitudes, and Conversion
Efficiency**

蔡敬康

Jing-Kang Chua

指導教授：戚務正 博士、龔源成 博士

**Advisors: Wu-Cheng Chi, Ph.D., Yuen-Cheng Gung,
Ph.D.**

中華民國 103 年 6 月

June 201

誌謝



不知不覺，自從大三暑假開始進入戚務政老師的實驗室已經過了三個寒暑。

在這期間遇到了很多的好老師和好同學，慢慢地引領著我進入科學研究的殿堂。原本地質科學系出生的我，對於地球物理的領域所知道的有如九牛一毛，還記得我人生中看的第一篇論文的第一張圖就是在工程界或是地球物理界裡無人不知，無人不曉的傅利葉變換，而我只能望之興歎。在地球物理的領域裡所有的基本概念都要重新學起，那一段路程是艱辛且孤獨的。

在上了一年龔源成老師的應用數學和地震學之後，我開始對地球物理領域有了一些基本的概念，期間也經歷了一段自學寫程式的痛苦歷程。然而這幾個基本的能力為我的畢業論文打下了一定的基礎。

我的第一個題目：Seafloor Compliance，幾乎快堅持了兩年，然而期間卻噩夢連連，在最後的半年裡幾乎天天處於崩潰且每晚睡覺都會被噩夢驚醒的狀態，我這非常鐵齒的人卻怎麼樣都不肯放棄，也非常感謝戚老師毅然決定要我換到了現在的題目（T-waves）。慶倖的是在之前磨練了快兩年的基本功一下子就發揮了出來，能夠在我念碩士班的兩年內順利畢業，深深感覺到了一個好的題目和好的基本功的重要。

最後我要特別感謝實驗室的大學姐陳利雯在這期間幫助了我很多，無論是研究上的或是生活上，沒有她我絕對沒有今天。謝謝她！

摘要



T 波是一種地震波相，其傳播路徑至少部份會經由水體介質傳播。這種聲速波可以傳至很遙遠的距離，因此更小規模的地震也能被偵測得到。但是目前對於控制 T 波的振幅和到時都還不甚了解。此研究希望能夠更了解 T 波經由固體地殼介質進入流體海洋介質的轉換點和在海洋中的傳播路徑。我們用了一顆海底地震儀和一個位於蘭嶼的陸域地震儀，在這兩顆地震儀共同的佈站時間記錄到了 60 個臺灣區域規模大於 3.3 的地震。其中這 60 個地震都有被海底地震儀接收到，另外只有大約 90% 的地震事件被蘭嶼的地震儀記錄到。我們利用這些被臺灣地震網精確定位的地震，去計算理論走時和理論 S 波-T 波，P 波-T 波的振幅轉換，結合了理論走時和理論振幅轉換，我們可以去模擬 T 波的振幅。模擬的 T 波波形與實際上觀測到的波形相符。從理論的到時，地震波的固體彈性波轉成流體聲速波的確與臺灣東部海域的海底地形有關，且我們觀察到部份 T 波波形缺口與地形的轉換缺口相吻合。最後我們也提出了一個全新的方法，利用地動訊號和海水壓力變化的比值，可去分辨海底地震儀接收到的 T 波是從海洋傳播抵達或是經由測站底下的地殼抵達。

關鍵字：T 波、T-波相、臺灣、海底地震儀、聲速波

Abstract



T-waves are seismic energies that have at least partially propagated through a water body. Such waves can propagate long distances, thus are useful for studying small events at far distances. However, factors controlling the amplitude and duration of T-waves are still not clear. It is also advantageous if we know where the energy enters into the water column and which parts of the T-wave is arriving from the crust or from the water column near the receiver side. Here, we used data from one broadband ocean bottom seismometer (OBS) that recorded T-waves from 60 $M_w > 3.3$ Taiwan earthquakes. T-waves from 90% of these events were also recorded by an island seismic station. For these earthquakes that are well-located by a dense land seismic network, we forward-calculated the travel times of the different parts of P- and S-wave convert to T-wave, and correlated them with different paths from the earthquakes. The duration of the observed T-wave fits with the paths from available conversion points in the regional bathymetry, and the waveform gap consistent to the gap of bathymetry contour. However, arrival times of a few abyssal earthquakes show that parts of the T-waves are converted directed from the deep seafloor near the sources. We have calculated the synthetic ground motions at the conversion points along the 1000 m bathymetric contour lines. We then calculated the synthetic T-wave amplitude at those conversion points. Using such results we calculated the T-wave amplitude envelopes and found that they can fit with the observed OBS data. Furthermore, we have used the ratio of ground motions to water pressure change to determine if the T-wave is arriving to the OBS as ground motions or as acoustic waves from the water column. Such method can help us to determine the different paths and amplitudes of the T-waves recorded by the OBSs.

Keywords: T-wave, T-phase, Taiwan, ocean bottom seismometer, acoustic waves



Table of Contents



誌謝	i
摘要	ii
Abstract.....	iii
Table of Contents	v
List of Figures.....	vi
List of Tables.....	vii
Chapter 1 Introduction.....	1
Chapter 2 Seismicity and Bathymetry of Taiwan Region	5
Chapter 3 Data Analyses	6
Chapter 4 Discussion	27
Chapter 5 Conclusions.....	31
Reference.....	33

List of Figures



Figure 1. Schematic T-waves propagation paths and Types.....	1
Figure 2. The seismic stations we used in this study region of Taiwan and the 60 events locations and mechanisms we have used.....	4
Figure 3. Event No. 46 recorded by S004, calculated P-T and S-T Type 1 T-waves traveltimes.....	10
Figure 4. The predicted T-wave amplitudes at the different conversion points (Event No. 46) from (a) P-wave and from (b) S-wave.....	13
Figure 5. Synthetic amplitude plotted with observed vertical seismic and water pressure.....	13
Figure 6. Event No. 27 recorded by S004, an example of observed Type 2 T-waves.	16
Figure 7. Event No. 46 recorded by S004, vertical seismic and water pressure change in time domain waveform and in frequency domain spectrogram, an example of ratios vertical seismic over water pressure change.....	17
Figure 8. Event No. 7 recorded by LYUB, calculated P-T and S-T Type 1 T-waves traveltimes.....	19
Figure 9. Two ways of conversions between crust and water column at the seafloor...	20
Figure 10. The ground acceleration over pressure-change ratios as a function of time for all the 60 events.....	21
Figure 11. Transfer function defined as the ratio between ground acceleration and water pressure changes.....	22
Figure 12. Two-way transfer function calculated as a function of the incident angle to the OBS.....	25
Appendix Figures	DVD

List of Tables

Table 1. 1D velocity model used for Green's function.....	7
Table 2. Event list from September 2006 to July 2007 in Taiwan region.....	8





Chapter 1 Introduction

T-waves [Linehan, 1940] are phases containing at least some acoustic paths through water bodies that are usually recorded by hydrophones, and sometimes by seismometers (Fig. 1).

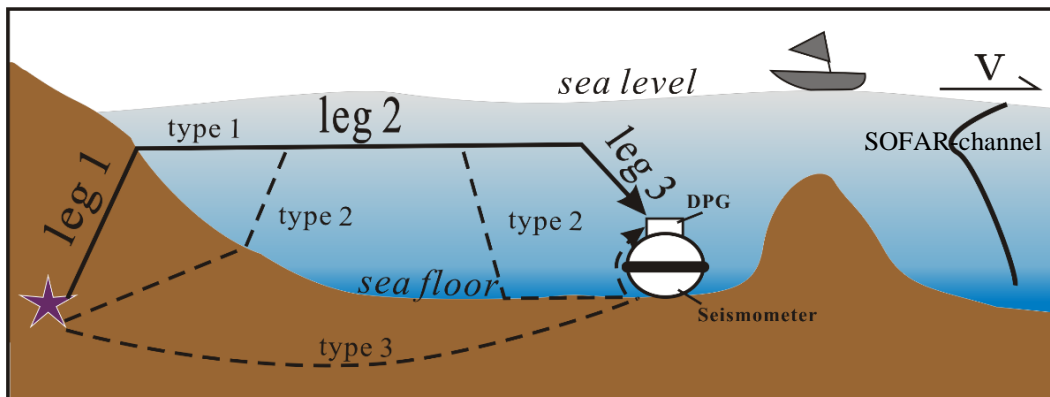
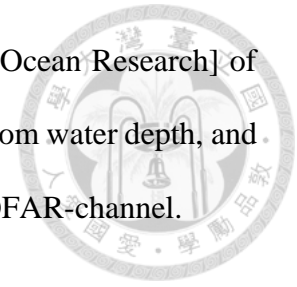


Figure 1: We have defined three different kinds of T-waves for this study. For the Type 1 T-wave, the first leg is the elastic wave from the earthquake to the conversion points at the 1000 m water depth. The second leg is traveling in the SOFAR-channel, a low velocity zone in the water column at around 1000 m water depth. See a cartoon of the water velocity profile to the right of the figure. The third leg is from the SOFAR-channel sub-vertically to the OBS. For the Type 2 T-wave, the first conversion point is outside of the 1000 m depth, or the second conversion point is far away from the OBS. For the Type 3 T-wave, the elastic wave propagates from the earthquake to the seafloor near the OBS. Then there is a shortest acoustic path to the OBS.

T-waves are important for studying abyssal earthquakes and also as an important monitoring tool for the Comprehensive Nuclear-Test-Ban Treaty. For the acoustic leg of the path, the energy in the ocean is mostly trapped at about a depth of 1000 m in the SOFAR (Sound Fixing and Ranging) channel, a low acoustic-velocity zone in the water column formed due to the decreasing temperature and increasing pressure at depth. *Okal* [2008] pointed out that rays can be trapped in the SOFAR-channel, which acts as a 2D wave-guide, instead of a typical 3D propagation in solid earth paths. In the impedance

data near to our S004 site provided by NCOR [National Center of Ocean Research] of Taiwan showed the slowest velocity in SOFAR-channel at 1000 m from water depth, and which heterogeneity might help to leak the T wave energy out of SOFAR-channel.



There is much less attenuation when energy travels in the SOFAR-channel, and T-waves of very smaller events from great distances can still be detected. The slow propagation velocity and the small attenuations in the SOFAR-channel makes it possible to better locate these events from afar. *Fox and Dziak* [1998] have used T-waves to successfully locate volcanic activity on Gorda Ridge, and helped a response cruise to the correct magmatic activity site. The detecting threshold for ridge events using T-waves is usually one magnitude below the seismic network [*J A Hanson and Bowman*, 2006].

Because earthquakes occur in solid earth materials, this implies that T-waves need to have at least one conversion between an elastic wave in solid earth and an acoustic wave in fluid, i.e. P or S to acoustic [*Okal*, 2008]. At the same time, acoustic to P [*D H Shurbet*, 1954] or S wave [*Okal and Talandier*, 1997; *D H Shurbet, and M. Ewing*, 1957] conversions have also been documented. Those studies have helped us better understand the T-waves.

However, there are debates on which part of the T-wave should be picked for relocation. Previously it was considered that beginning of the T-phase should be picked to satisfy the principle of causality, even though the emergent features of some T-waves made it difficult. On the other hand, using well-located events through typical seismological methods, it has been found that the traveltimes estimated using T maximum phases gave closer fits [*Fox and Dziak*, 1998; *J Hanson et al.*, 2001; *Slack et al.*, 1999]. In addition, there is no systematic study of how the radiation patterns of the earthquake affect the T-wave amplitudes. Without a better understanding of these issues, we can not

study the duration and the amplitudes of the T-waves in greater details. We also need to know the paths of the different parts of the T-waves before we can better relocate the events.



Accurate locations of earthquakes in remote abyssal regions are usually difficult to derive using other methods, thus it is usually difficult to calibrate the accuracy of the T-wave derived earthquake locations. The situation is also complicated by the trade-offs between origin time, depth, and location [Butler, 2006].

It will be helpful to study an earthquake which is well located by other methods, then pick different parts of the T-waves to see which phase in T-waves should be picked for relocation purpose. In addition, if there are many earthquakes with well-constrained focal mechanisms, we can also study the effects of earthquake radiation patterns on the T-wave attributes.

Whether P- or S-waves are more effective to be converted into T-waves is still under debate. *de Groot-Hedlin and Orcutt* [2001] suggest that, at low angles of incidence, the shear waves are mainly reflected back into the crust. Compressional waves are mainly reflected back into the crust at high incidence angles, with a smaller portion refracted into the sediments. Intuitively, the effective of converted T-waves are depended on seismic P- and S-waves normal vibration vector on seafloor. *Balanche et al.* [2009] suggest such a result using wave propagation simulations [Park et al., 2001]. They found that S-waves are more efficient than P-waves in producing energetic T-waves.

Here we systematically studied 60 $M_w > 3.3$ earthquakes in Taiwan region, all of which have excited T-waves. We used an ocean bottom seismometer (OBS) and a broadband seismic station on an island (Fig. 2) to study these earthquakes. For this study we use many earthquakes with well-constrained focal mechanisms to study the effects of

earthquake radiation patterns on the T-waves attributes. We study the effects of spatial gaps in conversion points on reducing the amplitude of the T-waves. We also propose a method to determine if the arriving T-waves energy is coming from water column or from the crust.

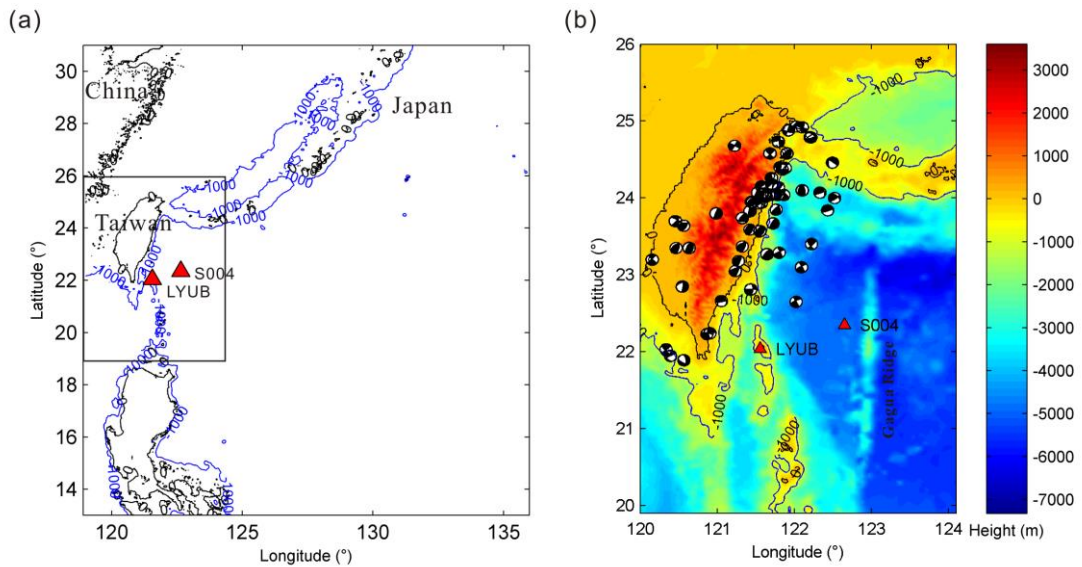
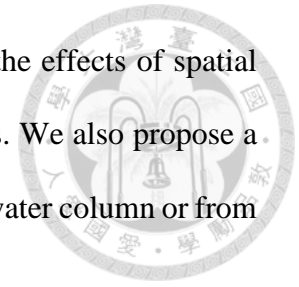


Figure 2: (a) The location map of Taiwan. Coast lines are shown with back color and 1000 m bathymetric contour lines with blue color. The red triangles are the locations of the OBS station (S004) and the island seismic station (LYUB); (b) Regional topography and bathymetry represented in color scheme and we also plotted the 60 earthquakes used in this study.

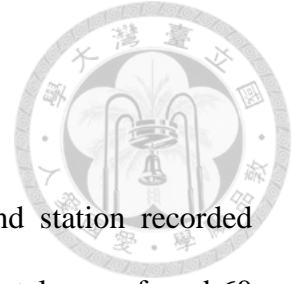
Chapter 2 Seismicity and Bathymetry of Taiwan Region



The island of Taiwan, covering an area of 36000 km², is among the most seismically active regions in the world. Most of the seismicity is a result of the collision between the Chinese passive margin and Luzon arc. Due to the extreme density of Taiwan's population, the seismicity is closely monitored by several very dense seismic networks. As a result, Taiwan is among the best seismically monitored regions in the world. The earthquake locations and focal mechanisms are well-constrained. The Central Weather Bureau of Taiwan routinely locates earthquakes [e.g. *Shin and Teng*, 2001]. The resolution of earthquake location is within 5 km for onland and coastal events. However, the error bound of the focal depths is harder to estimate. In addition, the Institute of Earth Sciences, Academia Sinica is routinely inverting high quality moment tensor solutions [e.g. *Kao et al.*, 1998]. On average, there are more than 70 moment tensor solutions derived annually. Such large amounts of high quality data provide a unique opportunity to study the relation between T-waves and earthquake source parameters.

The same collision processes also generate steep topography. Many earthquakes occur along the east coast of Taiwan where bathymetric slopes are very steep. The bathymetry of the abyssal plain then becomes relatively flat until a bathymetry ridge (Gagua Ridge) (Fig. 2b) near the eastern edge of our study region. The relatively flat bathymetry in the deep sea-basin east of Taiwan reduces the complexity of this study. Due to the finite length of the conversion points along 1000 m contour line in this region, it is possible to study the relation between the conversion points and the duration of the T-waves.

Chapter 3 Data Analyses



We have analyzed waveforms from an OBS and an island station recorded between September 2006 and July 2007. From the moment tensor catalog we found 60 $M_w > 3.3$ earthquakes occurred during this period. All of the 60 earthquakes have generated T-waves and are recorded by the OBS (Fig. 2). About 90% of the earthquakes have generated clear T-waves recorded by an island station.

The OBS (S004) contains a Guralp CMT-3TC seismic sensor with flat response between 20 Hz to 120 sec. Quanterra Q330 is used as the data logger, with sampling rate 40 sps. The sensor is decoupled from the OBS mainframe, and is leveled periodically during the deployment by a gimbal system with brakes [Thwaites *et al.*, 2005]. There is also a differential pressure gauge (DPG) mounted on each OBS's frame [Cox *et al.*, 1984]. The DPG is acting as a hydrophone at a 20 Hz sampling rate.

The island station LYUB contains a broadband seismometer with flat response between 20 Hz to 120 sec. Quanterra Q330 is used as the data logger, with sampling rate 40 sps.

In order to study different paths and conversion points of T-waves, we classify T-waves into 3 different types (Fig. 1). Type 1 represents direct seismic wave to acoustic wave conversion at SOFAR-channel, a low acoustic-velocity zone in the water column formed due to the decreasing temperature and increasing pressure at depth. Type 2 has at least 2 conversions between elastic waves and acoustics waves. Type 3 has only one conversion point near the OBS station.

For the Type 1 acoustic leg, the energy in the ocean leg is mostly trapped at about a depth of 1000 m in the SOFAR-channel. Type 2 either later than Type 1 enter to SOFAR-channel or earlier leakage from SOFAR-channel, in the result Type 2 stay longer in crustal propagation make it travel faster than Type 1 in a same profile. Type 3 T-waves have the shortest acoustic legs in the all kinds of T-waves. They are least studied or neglected because it is always contaminated with seismic P- and S- phases.

To calculate the travel times for Type 1 T-wave, we first assumed T-wave energy travels in three legs (Fig. 1): (1) solid earth seismic elastic wave with a regional 1D crustal velocity model [Table 1; *Rau and Wu, 1995*]; (2) horizontal hydroacoustic wave in SOFAR-channel at a water depth of 1000 m with a velocity of 1.48 km/s from a conversion point to directly above the OBS; and (3) a vertical path with a velocity of 1.5 km/s down to the OBS. The first leg was calculated using a Tau-P method [*Crotwell et al., 1999*].

Table 1. 1D velocity model used for Green's function

Thickness (km)	Depth (km)	V _p (km/s)	V _s (km/s)	Density (g/cm ³)	Q _p	Q _s
2.2	2.2	4.5	2.6	1.8	200	100
2.2	4.4	4.85	2.8	2.05	600	300
2.2	6.6	5.3	3.06	2.25	600	300
2.2	8.8	5.6	3.23	2.39	600	300
4.5	13.3	5.84	3.37	2.5	600	300
4.5	17.8	6.13	3.54	2.64	600	300
7.5	25.3	6.28	3.63	2.7	600	300
8.5	33.8	6.6	3.81	2.85	600	300
5	38.3	6.87	3.97	2.97	600	300
21.5	60.3	7.43	4.29	3.3	600	300
25	85.3	7.8	4.5	3.3	600	300

Assuming different parts of the T-wave for this particular earthquake Event No. 46 (see Table 2) are associated with paths of different convergent points, we calculated

the total travel time associated with one particular conversion point on the seafloor. Similar calculations were performed for thousands of conversion points along the 1000 m contour line offshore Taiwan, and plotted in Figure 3. We have done similar analyses for all the 60 earthquakes (see Fig. 3 and Appendix). OBS waveforms from the earthquakes show clear T-waves, especially after a bandpass filter of 1 to 9 Hz. The durations of the T-waves ranges from 100 to 200 sec.

Table 2. Event list from September 2006 to July 2007 in Taiwan region

Event No.	Year	Julian day	Hour	Min.	Sec.	Lat.	Log.	Depth (km)	Mw
1	2006	257	20	47	34.6	24.93	122.02	87	4.01
2	2006	258	20	54	36.37	24.15	121.57	18	3.61
3	2006	262	13	0	5.72	24.68	121.22	12	3.27
4	2006	273	6	49	28.19	24.46	122.49	80	4.15
5	2006	274	6	36	17.67	24.03	121.62	19	4.38
6	2006	281	11	42	43.43	23.83	121.42	32	3.78
7	2006	282	0	44	25.32	24.02	121.63	22	3.79
8	2006	285	14	46	29.9	24	122.52	23	5.47
9	2006	316	2	40	59.3	23.94	121.57	44	4
10	2006	317	22	29	27.4	23.4	122.22	12	4.31
11	2006	320	1	50	19	23.1	122.09	19	4.54
12	2006	329	8	54	55.1	23.93	121.53	12	3.4
13	2006	330	19	46	10.7	24.04	121.7	44	3.82
14	2006	339	22	36	1.2	24.26	121.7	21	4.14
15	2006	340	1	36	9.6	23.85	121.76	33	3.64
16	2006	348	11	10	32.9	24.92	122.1	32	4.57
17	2006	351	13	42	13	23.94	121.45	24	3.94
18	2006	352	3	47	28.1	23.95	121.44	26	3.43
19	2006	352	14	32	12.9	24.07	121.52	18	3.37
20	2006	353	20	44	36.5	24.79	122.2	11	4.28
21	2006	357	17	28	29.3	24.79	122.21	12	4.84
22	2006	360	8	20	4.5	23.37	121.32	17	3.93
23	2007	14	5	55	2.8	24.06	121.61	19	3.55
24	2007	16	3	10	35	23.84	122.43	21	4.93
25	2007	17	4	0	25.9	24.04	121.86	32	4.02
26	2007	20	11	48	11.7	23.2	120.15	13	3.45
27	2007	25	10	59	12.4	22.65	122.02	20	5.69
28	2007	31	2	16	58.4	23.35	120.46	13	3.36
29	2007	36	9	17	46.2	24.1	122.1	50	3.56
30	2007	43	5	40	25.2	24.4	121.81	16	3.59
31	2007	45	3	26	16.7	22.23	120.86	12	4.38
32	2007	45	3	30	31	22.24	120.9	13	4.52
33	2007	53	21	0	16.4	24.14	121.79	15	4.05
34	2007	58	19	57	10.4	24.04	121.78	30	3.9

35	2007	66	22	57	17.2	24.07	122.33	26	4.86
36	2007	67	15	37	37.1	24.58	121.9	71	4.08
37	2007	71	13	35	51.7	24.18	121.7	12	4.33
38	2007	82	18	23	0.5	23.05	121.23	16	3.96
39	2007	86	5	16	38.9	23.35	120.63	16	3.5
40	2007	90	2	45	6.4	24.88	121.92	83	3.78
41	2007	115	17	11	53.9	23.29	121.8	28	3.91
42	2007	117	11	1	55.7	23.7	120.45	16	3.33
43	2007	130	11	11	46.6	23.8	120.98	26	3.31
44	2007	132	17	50	11.4	24.58	121.68	41	3.97
45	2007	152	3	51	20.1	22.81	121.43	24	3.91
46	2007	166	20	29	13.4	23.27	121.64	25	4.08
47	2007	168	4	26	22.3	24.39	121.88	15	3.35
48	2007	175	14	38	48.1	22.85	120.54	18	3.44
49	2007	177	14	47	34.1	23.18	121.27	14	3.36
50	2007	184	11	55	44.3	23.74	121.32	26	3.55
51	2007	193	20	54	13.1	24.73	121.79	23	4.06
52	2007	197	23	42	52.6	23.57	121.55	24	4.38
53	2007	198	22	42	31.2	23.59	121.42	28	3.63
54	2007	200	5	56	14.5	23.64	120.56	16	3.21
55	2007	202	22	55	23.1	24.37	121.84	25	3.57
56	2007	204	13	40	2.1	23.67	121.72	29	5.07
57	2006	360	12	26	24.9	21.89	120.56	41	6.7
58	2006	360	12	34	14.83	21.9463	120.387	30	6.54
59	2006	361	2	30	39.7	22.03	120.33	30	5.28
60	2007	221	0	55	47.8	22.66	121.05	21	5.09

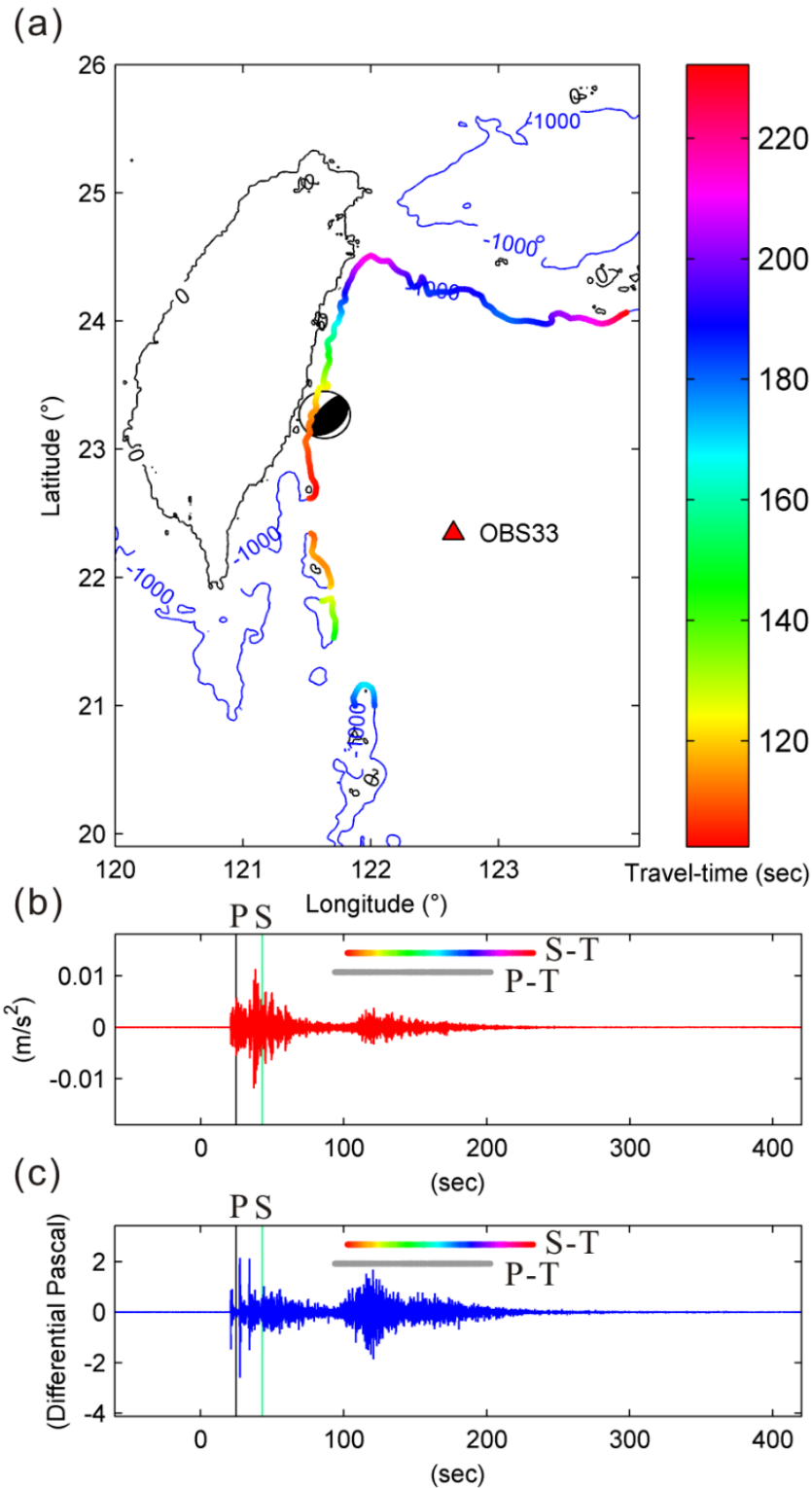
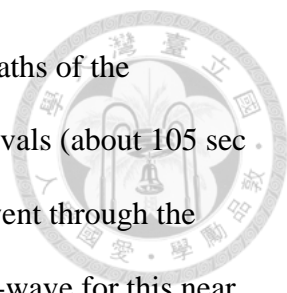


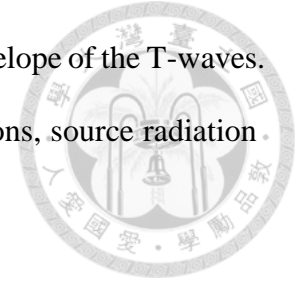
Figure 3: T-wave generated by a thrust event (No. 46 in Table 1) near Hualien. (a) The color scheme plotted on the 1000 m bathymetry contour represents the combined S-T travel time in three legs; (b) Vertical seismic and (c) DPG waveforms have been band-pass filtered between 1-9 Hz. Again color bar represents the combined S-T travel time, and the gray color bar represents the combined P-T travel time. The black and green vertical lines depict the P and S arrival times, respectively. The observed duration of Type 1 T-waves are consistent with our predicted combine P-T and S-T arrival times and duration.



The arrival time and duration of the T-wave coincide with the paths of the available P-T and S-T conversion points in this region. The early arrivals (about 105 sec of total traveltime) of T-wave have the P to T and S to T paths that went through the conversion points near latitude 22.5° N. The large amplitude of the T-wave for this near coast event arrived about 125 sec after the origin time, and had the short seismic elastic path, i.e. the conversion point is closer to the earthquake. The later phase (between 140 and 160 sec of travel time, green color) is more complicated because there were two paths: one with a conversion point at a latitude of 21.7° N, and another at 23.7° N. For the phases that arrive between 170 and 190 sec, there are three different paths: one with the conversion point at 21° N, another at 24.2° N, and the third one also at 24.2° N but at a longitude of 122.5° E, instead of 121.7° E. The latest arrivals (200-220 sec, neon color) are associated with furthest conversion points at 124° E and conversion points at 24.5° N, 122° E.

The complexity of the different paths from multiple conversions arriving at the same time is due to the geometry of the 1000 m contour line and the locations of the earthquake and the OBS. Some of the P and S waves propagate to the north, then converted to a T-wave to propagate back to SE. Such a path configuration made the arrival time increase dramatically for conversion points to the north. However, as the 1000 m contour line turns right near to the 24.6° N, the travel time started to decrease even though the conversion point was farther away. This is due to a shorter SOFAR path in which the propagation velocity is slower compared with that of the elastic waves. For convergent points further to the east, the increasing length of the elastic wave path finally took stronger effect, and increased the travel times. Overall, our model with the multiple paths from different conversion points can predict the duration of the T-wave.

Next we want to study the factors affecting the amplitude envelope of the T-waves. The factors we want to examine include the elastic wave propagations, source radiation patterns, and the availability of the conversion points.



In order to synthetic Type 1 T-wave amplitude, we have used the FK code [Zhu and Rivera, 2002] and a Taiwan average 1D crustal velocity model to generate synthetic displacement ground motions using the moment tensor source parameters. The displacement waveforms then were converted into acceleration waveforms (Fig. 4). We have done this at the thousands of conversion points along the 1000 m contour line. Such calculations were done for all the 60 earthquakes in this study. We then calculated the inner product of the peak accelerations in the P and S wave time windows with a unit vector that is normal to the bathymetric slope at the conversion points. The time windows for P and S waves are starting with their theoretical arrival times with durations of 2 and 5 seconds, respectively. The short time window for P is to exclude S wave when the S-P time is short. We will treat the inner product as the peak amplitude of the acoustic wave that comes into the SOFAR-channel from that particular conversion point. We do not consider the T-wave attenuation in the SOFAR-channel due to the relatively short propagation distances for these earthquakes. We then can associate the amplitude to the arrival time. We have summed the P and S amplitudes together to derive a synthetic T-wave amplitude envelope. Such envelope then is compared with the envelopes derived from the DPG and the BHZ components (Fig. 5). The envelopes are smoothed using an 8 sec moving window.

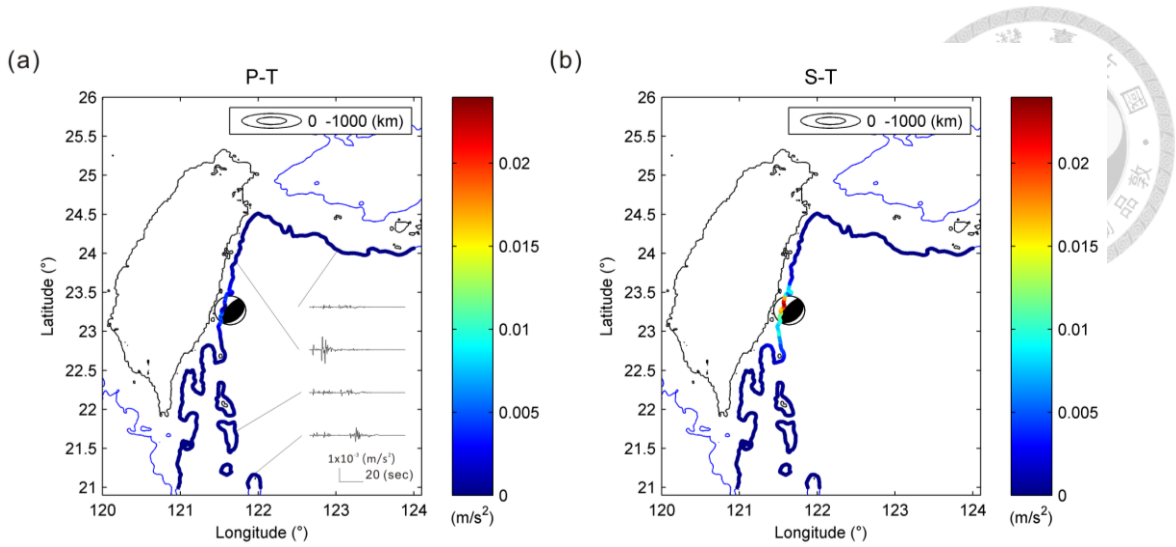


Figure 4: The predicted T-wave amplitudes at the different conversion points (Event No. 46) from (a) P-wave and from (b) S-wave. We have calculated the synthetic ground motions at each convergent points along the 1000 m contour lines. Vertical and horizontal scales represent 1×10^{-3} (m/s²) and 20 (sec), respectively. First we calculated the maximum P and S wave vector sums from the synthetic waveforms. Next we calculated the inner product of the P and S vector sums with the unit vector that is normal to the bathymetry in order to get the predicted T-wave amplitudes. Note that in this case, and in most of the other cases, S to T conversion generates

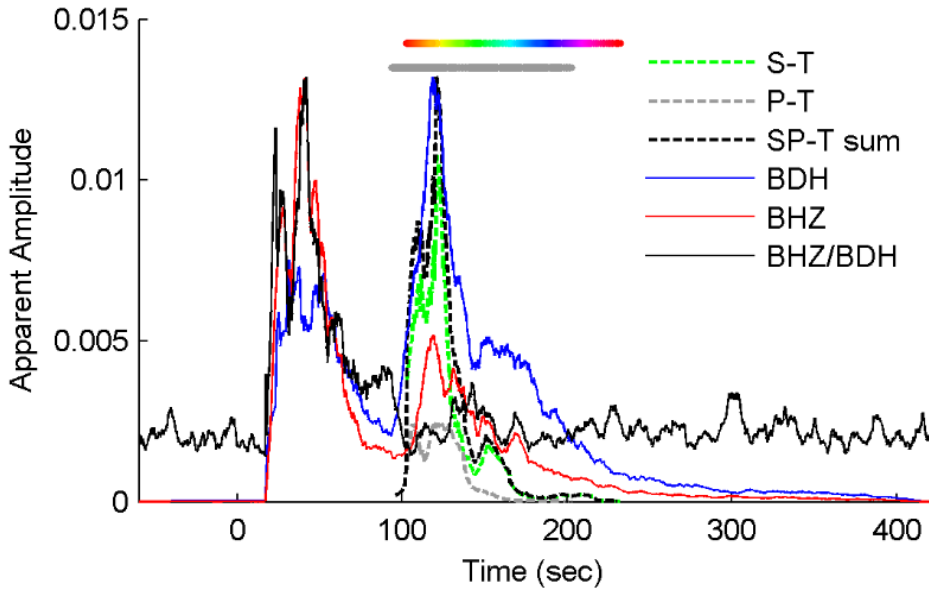
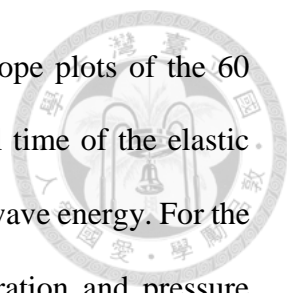


Figure 5: We have plotted the amplitude envelopes of vertical ground acceleration (red) and DPG (blue) for the Event No. 46. The P-T synthetic conversion associated with traveltime is plotted in gray dashed line, and S-T in green dashed line. We then plotted the sum of both P-T and S-T conversion in black dashed line. We can fit the overall amplitude envelope to the first order. Some of the reduced T-wave amplitude (at 110 sec and 150 sec) are due to the gaps in the 1000 m contour lines in this region. The color and gray bars are the predicted travel time for the Type 1 S-T and P-T in this region. Note also the ratio between ground acceleration and water pressure changes (black line) are different during the arrival time of the P and S waves, and the arrival time of the T-wave. The observed amplitude envelopes are smoothed using an 8 sec moving time window.



There are usually two energy pulses in the amplitude envelope plots of the 60 events that we studied. The first pulse is associated with the arrival time of the elastic wave phases, while the second pulse is associated with that of the T-wave energy. For the first pulse, the ratio between the observed vertical ground acceleration and pressure changes is larger than that in the second pulse (Fig. 5). In our simulation of P to T and S to T conversions, both have contributed on the durations and amplitudes of recorded waveforms. However, the S waves generally generate stronger T-waves. In later part (150 sec after the origin time) the predicted T amplitude decrease for a while before resuming back to larger amplitude. This is due to the gap in the 1000 m contour line in this region, between the latitudes of 22.2° N and 22.5° N (Fig. 3). Such pattern can also be found in the observed data, in both the vertical ground acceleration and the pressure changes (Fig. 5). This demonstrates the efficiency of the conversion points at 1000 m water depth for exciting strong T-waves.

Not all the T-waves are excited by the conversion points along the 1000 m contour line. Next we will show T-waves excited by an abyssal earthquake that is far away from the 1000 m bathymetry contour line. From the traveltimes analysis (Fig. 6) we found some T-wave energy arriving before the predicted P and S to T conversion at the 1000 m contour line. This suggests that there is T-wave energy that has shorter acoustic path than the Type 1 T-wave. By definition this means that there is Type 2 T-wave energy observed for such an abyssal earthquake. We have calculated the travel time for the path that goes from the earthquake to the hypocenter, then to the SOFAR-channel before going down sub-vertically to the OBS site. Such T-wave can also be identified in DPG (Fig. 6c). We see increase T-wave energy at this arrival time (Fig. 6c & d), especially on the DPG channel. Note that there is still an increase of the T-wave amplitude in the predicted P and S to T conversion at 1000 meter contour line. To sum, this demonstrated that it is

possible for T-wave energy to enter into the water column not only at 1000 m bathymetric contour lines but also at any points on the seafloor.



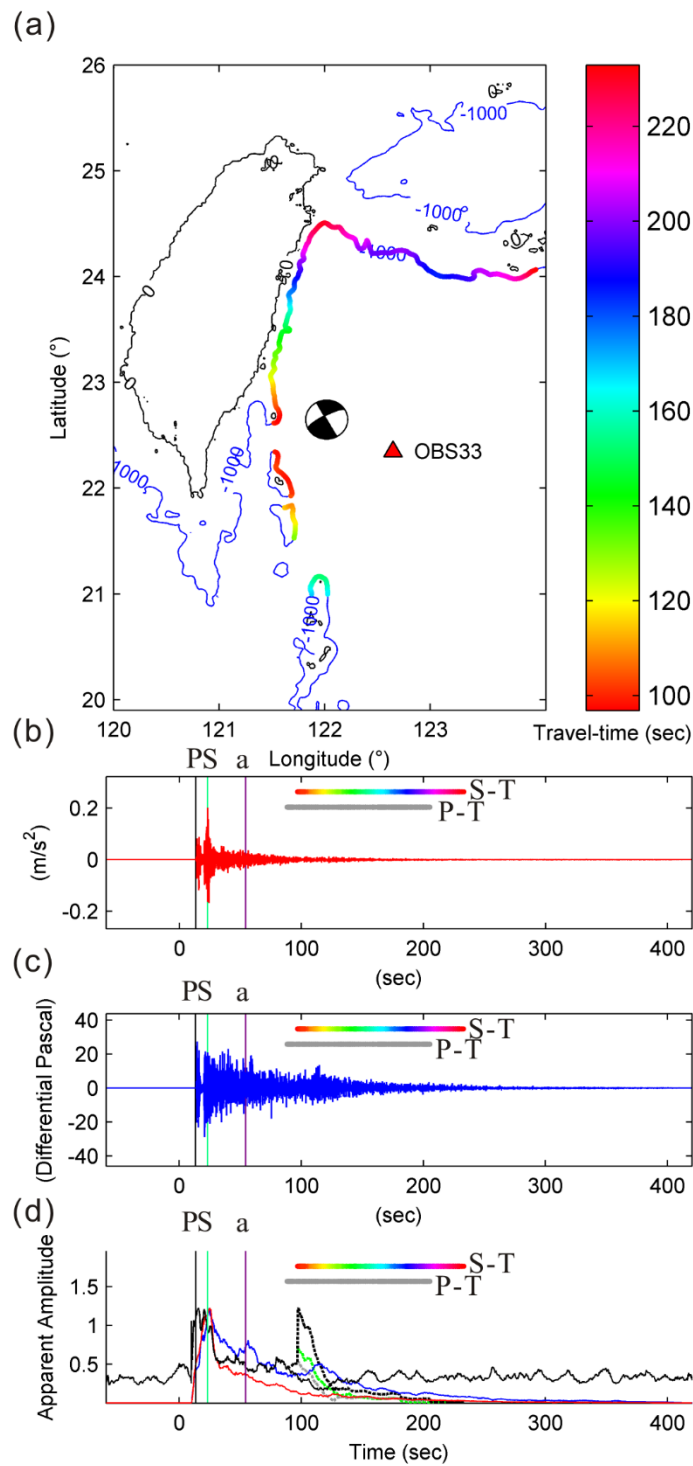


Figure 6: An example of T-waves excited by an abyssal earthquake (Event No. 27). (a), (b) and (c) same as the configuration in Fig. 3; (d) same as the configuration in Fig. 5. We interpret that there are some T-wave energy arriving from the water column to the OBS starting at 25 second after the earthquake origin time, based on the barely decayed signal after S-phases. We also calculated the travel time for a path with a SOFAR-channel leg from the above the earthquake to above the OBS, and marked the time as “a” with purple vertical line. It coincides with a time when we see an increase of apparent water pressure change in (c) and (d). We also see an increase of T-wave energy at the arrival time of the Type 1 T-wave.

Next we show an example of the Type 3 T-wave using the same event used in Figures 3, 4 and 5. We have plotted the spectrograms of the vertical ground acceleration and pressure changes (e.g. Fig. 7, and Appendix). In Figure 7, the first pulse of the T-wave energy is correlated with the elastic wave arrival times at the OBS site. The DPG also recorded water pressure changes at the same time. Usually we see strong energy at frequency bands between 6 and 8 Hz in the ground motions. For the BDH channel, we see stronger energy between 2 and 6 Hz. Overall, weak T-wave energy can be seen between 1 and 10 Hz. It has higher ground acceleration to pressure change ratio compared with the second pulse of the T-wave energy that fits with the Type 1 T-wave travel time (Fig. 7e). Such feature can be observed in all the 60 events we have studied (see Appendix). In later section we will analyze the possible mechanism for such change of ratio between Type 1 and Type 3 T-waves.

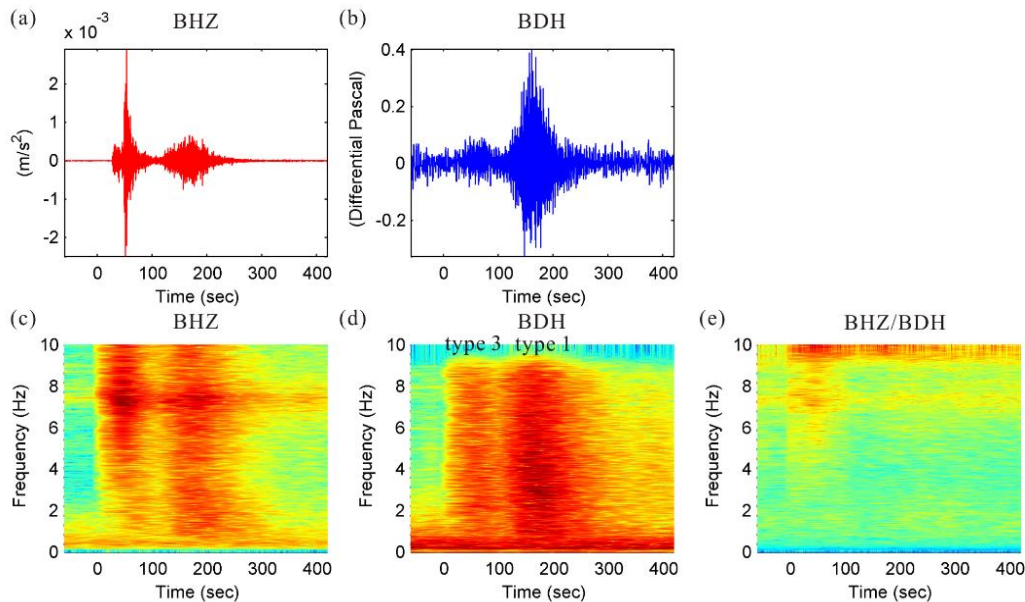
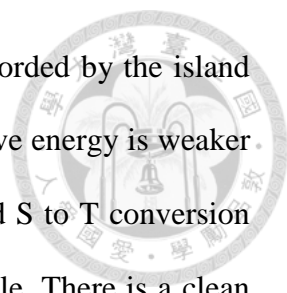


Figure 7: Waveforms of the (a) acceleration ground motions and (b) DPG for Event No. 46. We have also plotted their frequency spectra (c) and (d) respectively, in addition to a transfer function defined as the (e) ratio of the acceleration over the pressure changes. We have marked Type 1 and Type 3 T-wave in (d). For the transfer function (e), its values are higher during the P- and S-waves, but lower during the T-wave.



For all the 60 events, we have also studied the T-waves recorded by the island seismic station. We found T-wave in about 54 events, and the T-wave energy is weaker than that in the OBS. We see T-wave energy in the predicted P and S to T conversion time window. Here we use an earthquake Event No. 7 as an example. There is a clean energy occurred in the predicted T-wave arrival time window (Fig. 8). And there is a gap in the T-wave energy, correlating to the conversion points between latitudes 22.6° N to 24° N. These conversion points do not have direct line of sight to the seismic station because part of the 1000 m contour line has blocked them. The first section predicted P to T arrival time is earlier than that of the S arrival. S-waves are always contaminated with first section of Type 1 T-wave, e.g. higher amplitude before S arrival and long duration. The shapes of the T-waves recorded by LYUB are very different. For earthquakes occur to the west of these conversion points, we also observe smaller or no T-wave energy. But earthquakes to the north of this shadow zone usually generate clear T-wave recorded by this island station.

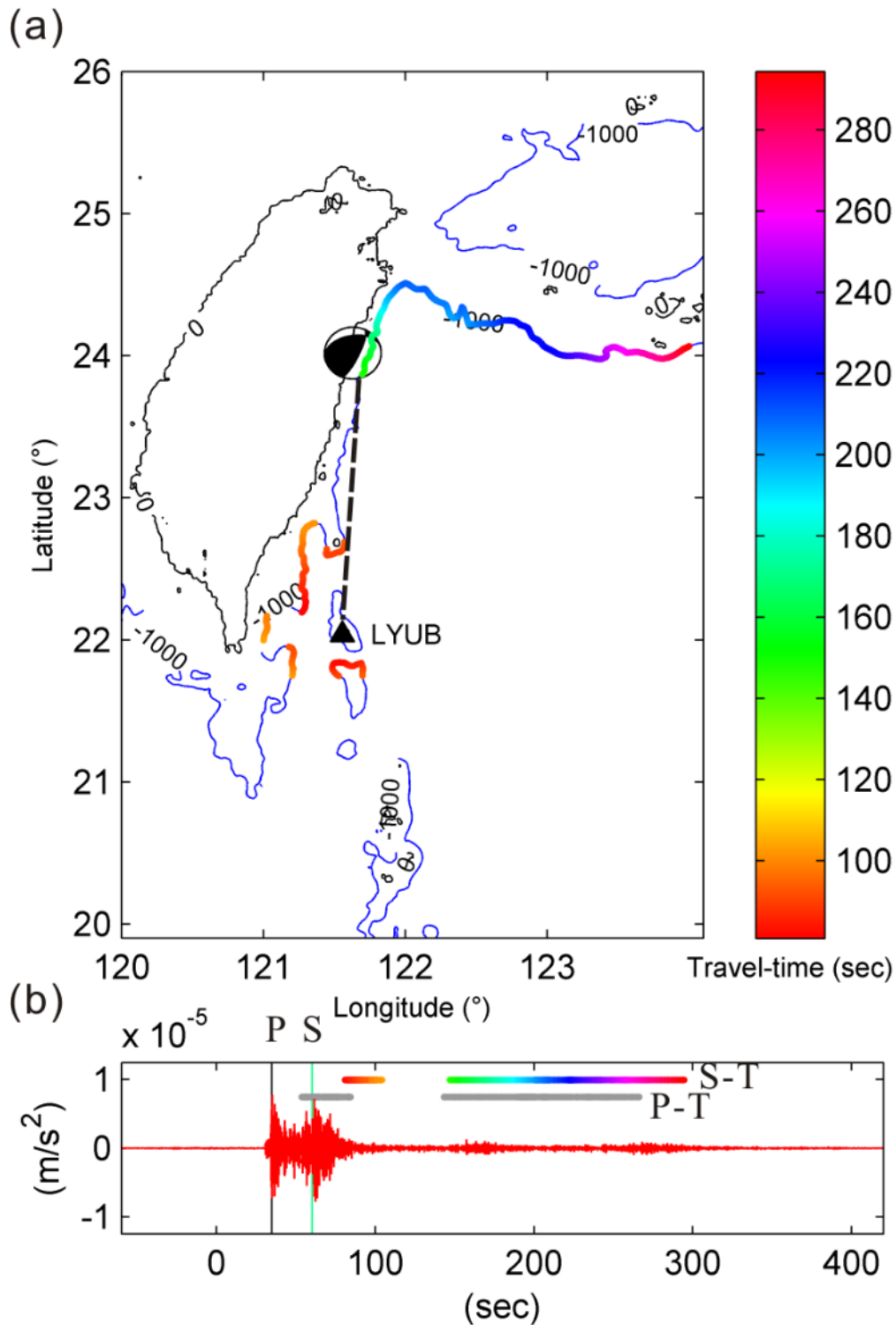
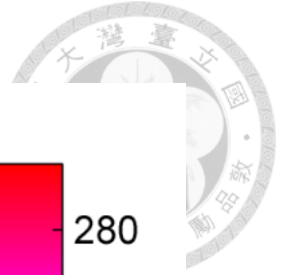


Figure 8: T-wave recorded by the island station LYUB (Event No. 7). The acceleration waveforms were filtered between 1 and 9 Hz. Note that the predicted P to T arrival time is earlier than that of the S arrival. There is a gap in the T-wave energy, correlating to the conversion points between latitudes 22.6° N to 24° N. These conversion points do not have direct line of sight to the seismic station, thus might need to have additional conversions, causing a weaker T-wave. We see similar effects for many earthquakes to the north.

It will be helpful if we can differentiate the main energy that arrives to the OBS from the water column (Type 1 and some Type 2) or from the crust (Type 3). Because the ground motion and water pressure energies arrive at the same time, such ambiguity makes travel path determination difficult. To solve this problem, we had developed a method to differentiate these two cases using a transfer function between the ground accelerations and water pressure changes.

Seafloor is an interface between sea water and solid crust (Fig. 9). These two materials have different modulus. Thus the conversion from acoustic to elastic should have different conversion efficiency than the elastic to acoustic conversion. We had observed that Type 1 and Type 3 T-waves have different ratios between vertical seismic component and DPG-component. If we applied Hooke's Law in Figure 9, that Type 1 and Type 3 T-waves have different ratios due to the different moduli between crust and sea water.

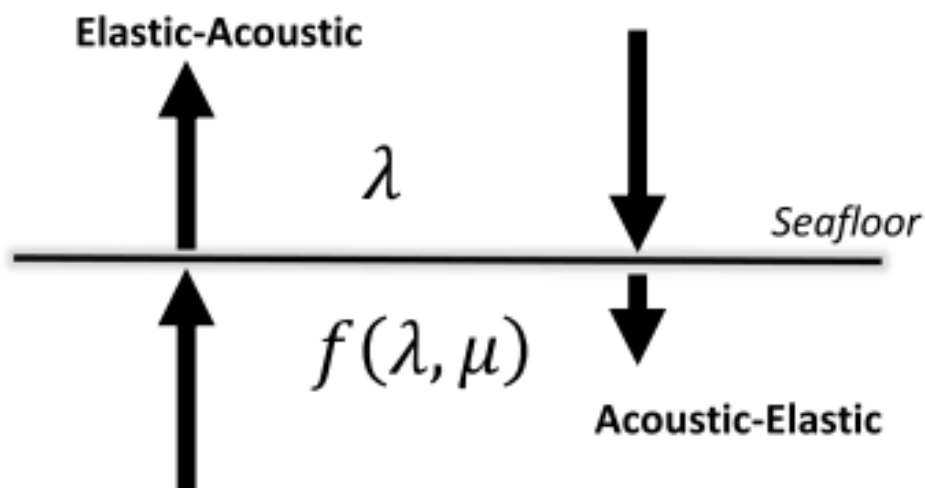


Figure 9: Two ways of conversions between crust and water column at the seafloor. Note that we have used a unit energy source while the amplitudes of the transmitted energy for the elastic to acoustic and acoustic to elastic might be different.

We have plotted the ground acceleration over pressure-change ratios as a function of time for all the 60 events (Fig. 10). We found higher ratios during the P-wave arrivals, and even higher ratios during the S-wave arrivals. However, the ratios during the Type 1 T-wave arrival times are generally low, the results ratios similar to the spectrum ratio in Figure 7e.

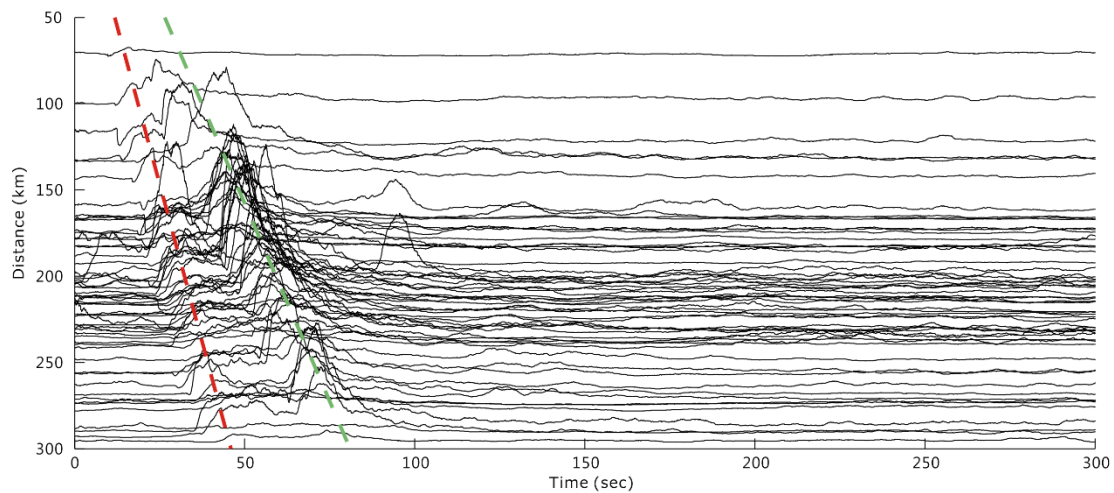
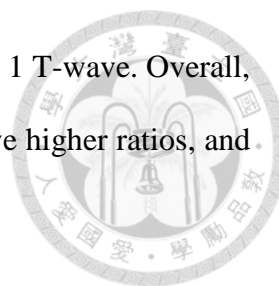


Figure 10: The ground acceleration over pressure-change ratios as a function of time for all the 60 events. The ratios have been normalized. The events are sorted according to the epicentral distance. We found higher ratios during the P wave arrivals, and even higher ratios during the S wave arrivals. However, the ratios for the Type 1 T-wave arrivals (not marked because they are not a function of the epicentral distance) are generally low.

All of the spectrograms of 60 events in our OBS station have showed this two different of ratios between two dominant energy pulses, one correlating with the elastic wave arrival times, while the other correlating with the Type 1 T-wave arrival time (Fig. 7 and Appendix). To further exam the ratio between elastic ground acceleration and acoustic pressure in time domain, we had plotted the ratios of all of the events in Figure 11. To choose the time windows of Type 3 P to T, S to T and Type 1 combined T-waves, we have chosen a three-second time window that is 0 to 3 sec after the first arrivals of the phases using the average absolute amplitudes of the OBS waveforms. We can see that



Type 3 P-T and S-T have wider ranges of ratios than that of the Type 1 T-wave. Overall, Type 1 T-wave has smaller ratios, while the average Type 3 P-T have higher ratios, and Type 3 S-T even higher.

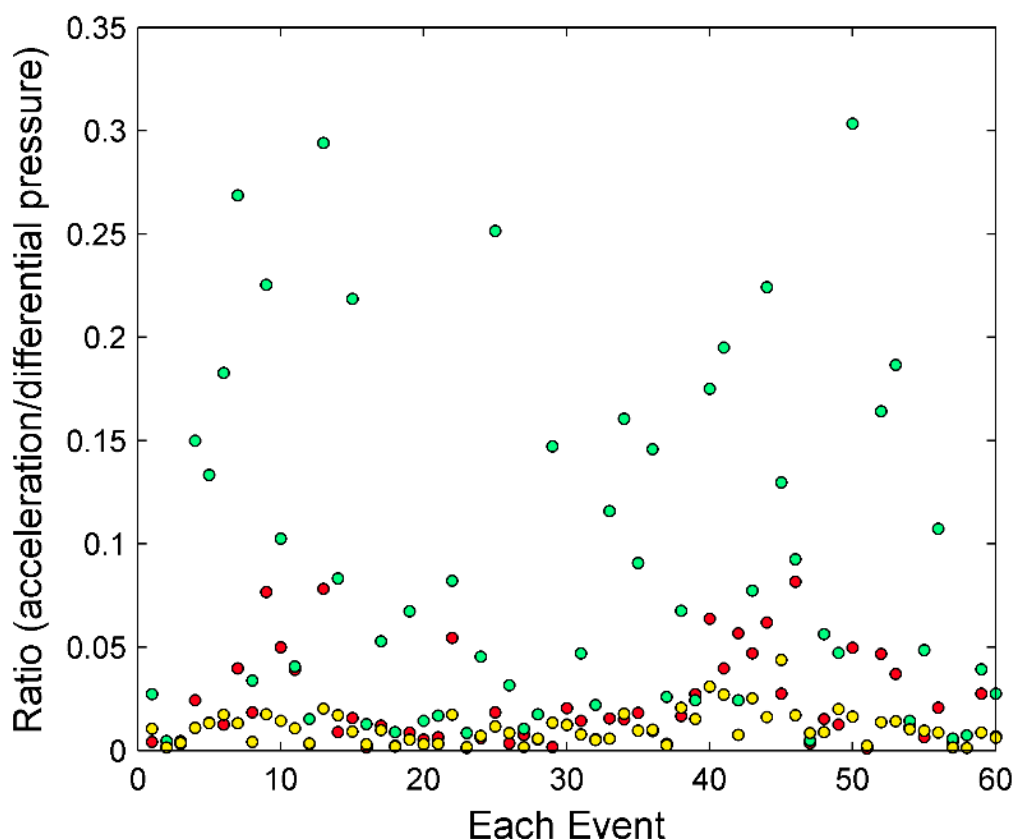


Figure 11: A transfer function defined as the ratio between ground acceleration and water pressure changes. We have studied 60 earthquakes, and plotted such transfer function for the time windows of the travel time P (red), S (green), and Type 1 T-waves (yellow). Note that the Type 1 T-wave has very small transfer functions, while the others have higher ones.

Based on Newton's second Law, forcing is directly proportional to the acceleration, so we use acceleration rather than velocity ground motions.

$$\Delta p = \rho h \Delta a \quad (1)$$

In our calculation in Figure 11, it may be written as an equation below.

$$\frac{a}{\Delta p} = \frac{a}{\rho h \Delta a} \quad (2)$$



Equation 2 gives a relation between observation and the physical insights. The left side of the equation can be derived from the observed seismic and DPG waveforms. Equation 1 shows that there might be a linear relationship between the differential pressure changes and the ground acceleration. And in the case of energy propagating from water column to the crust (Type 1 T-wave), the left side has a dimension similar to a kind of transfer function called the seafloor compliance [e.g. *Crawford et al.*, 1991], in which the source is in the denominator while the response is in the numerator. This ratio is relatively constant for Type 1 T-wave. For the case of wave propagating from the crust to the water column at the OBS site, as the case of Type 3, the left side implies that the source is in the numerator while the response is in the denominator. The ratio between the ground acceleration and the water pressure changes becomes another type of transfer function. Figure 11 shows that most of the acceleration over pressure change ratios range between 0.005 to 0.02 for Type 1, 0.01 to 0.1 for Type 3 P-T and 0.01 to 0.3 for Type 3 S-T, respectively.

Next we can derive a dimensionless parameter that we have informally called two-way transfer function. It is defined as the quotient of the two ratios, i.e. two transfer functions, across the fluid and elastic interface. The numerator of the quotient is the ratio of the ground acceleration over the pressure for Type 3 T-wave. The denominator is the same ratio for Type 1 T-wave. The two-way transfer function is related to the moduli of the fluid and the solid across the interface.

For a Type 3 P to T conversion, the ratio of the ground motion amplitude over the acoustic wave amplitude in the water is:

$$\frac{1 + \overset{\diagup}{P}\overset{\diagdown}{P} + \overset{\diagup}{P}\overset{\diagdown}{S}}{\overset{\diagup}{P}\overset{\diagup}{P}} \quad (3)$$



For a Type 3 S to T conversion, the ratio of the ground motion amplitude over the acoustic wave amplitude in the water is:

$$\frac{1 + \overset{\diagup}{S}\overset{\diagdown}{P} + \overset{\diagup}{S}\overset{\diagdown}{S}}{\overset{\diagup}{S}\overset{\diagup}{P}} \quad (4)$$

For a Type 1 T to P and S conversion, the ratio of the ground motion amplitude over the acoustic wave amplitude in the water is:

$$\frac{\overset{\diagdown}{P}\overset{\diagdown}{P} + \overset{\diagdown}{P}\overset{\diagdown}{S}}{1 + \overset{\diagdown}{P}\overset{\diagup}{P}} \quad (5)$$

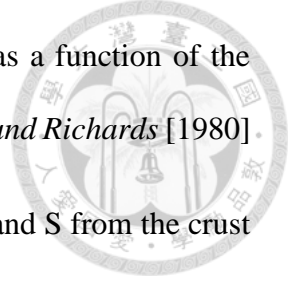
The “1” in equation refers to the unit amplitude of the incident T-wave.

Two-way transfer functions of the P-wave, equation 3 over equation 5:

$$\frac{\frac{1 + \overset{\diagup}{P}\overset{\diagdown}{P} + \overset{\diagup}{P}\overset{\diagdown}{S}}{\overset{\diagup}{P}\overset{\diagup}{P}}}{\frac{\overset{\diagdown}{P}\overset{\diagdown}{P} + \overset{\diagdown}{P}\overset{\diagdown}{S}}{1 + \overset{\diagdown}{P}\overset{\diagup}{P}}} \quad (6)$$

Two-way transfer functions of the S-wave, equation 4 over equation 5:

$$\frac{\frac{1 + \overset{\diagup}{S}\overset{\diagdown}{P} + \overset{\diagup}{S}\overset{\diagdown}{S}}{\overset{\diagup}{S}\overset{\diagup}{P}}}{\frac{\overset{\diagdown}{P}\overset{\diagdown}{P} + \overset{\diagdown}{P}\overset{\diagdown}{S}}{1 + \overset{\diagdown}{P}\overset{\diagup}{P}}} \quad (7)$$



From Figure 12 we plotted the two-way transfer functions as a function of the incident angle to the OBS. We use a convention similar to that of *Aki and Richards* [1980] to define the incident P from the water column to be $\overset{\frown}{P}$; incident P and S from the crust to be $\overset{\frown}{P}$ and $\overset{\frown}{S}$. For the converted waves, the down-going P in the water column can convert to $\overset{\frown}{P}\overset{\frown}{P}$, $\overset{\frown}{P}\overset{\frown}{S}$ and $\overset{\frown}{S}\overset{\frown}{S}$, and up-going P and S in the crust can convert to $\overset{\frown}{P}\overset{\frown}{P}$, $\overset{\frown}{P}\overset{\frown}{S}$, $\overset{\frown}{S}\overset{\frown}{P}$, $\overset{\frown}{S}\overset{\frown}{P}$ and $\overset{\frown}{S}\overset{\frown}{S}$. For example, S incident from the crust will generate $\overset{\frown}{S}\overset{\frown}{P}$, $\overset{\frown}{S}\overset{\frown}{P}$ and $\overset{\frown}{S}\overset{\frown}{S}$.

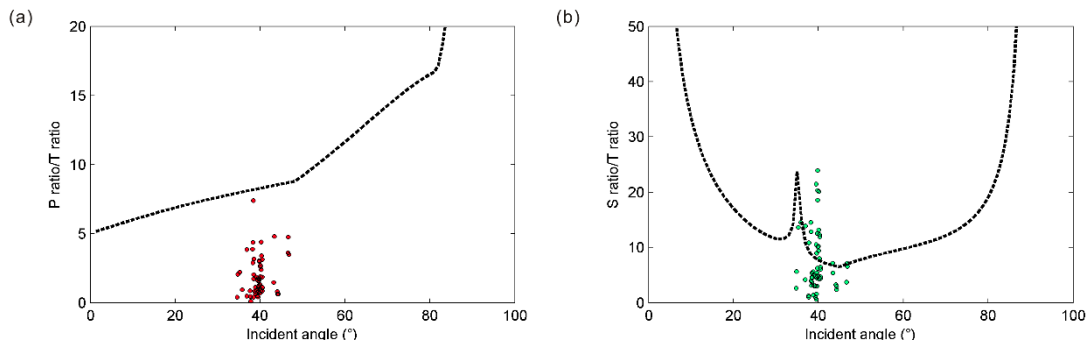
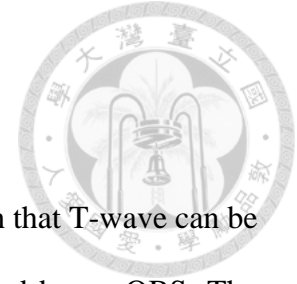


Figure 12: Two-way transfer function calculated as a function of the incident angle to the OBS. The two-way transfer function is defined as the quotient of two ratios. The numerator of the quotient is the ratio of the ground acceleration over the pressure for Type 3 T-wave from (a) P wave (Equation 6) and (b) S wave (Equation 7). The denominator is the same ratio for Type 1 T-wave. The circles are derived from the observed data. We see a better fit in (b).

The reflection and transmission coefficients are a function of the crustal P and S velocities, crustal density, water velocity, water density, and the incidence angle. Here we use a half space crustal velocity model the top layer of the 1D velocity model by *Rau and Wu* [1995], and the water velocity we used at 1.5 km/s, water density at 1.075 g/cc. The calculated incident, reflected, and transmitted wave amplitudes then were used to calculate the ratios of ground motions over the water pressure for Type 3 and Type 1 T-waves. After that, we can derive the two-way transfer function as a function of the

incident T-wave angle for the Type 3 T-wave. The incident angles to the OBS are calculated from 1D crust velocity model of *Rau and Wu* [1995]. For the Type 1 T-wave, the incident angle is always assumed to be zero because we assume that most of the energy comes down sub-vertically from the SOFAR-channel. The predicted two-way transfer functions better fit the observed data in Type 3 S-T over Type 1 T-wave ratios than Type 3 P-T over Type 1 T-wave ratios (Fig. 12), although there is still a wide spread of data points.

Chapter 4 Discussion

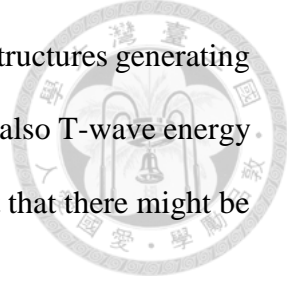


The earthquakes and the bathymetry in Taiwan regions are such that T-wave can be excited by relatively small ($M_w > 3.3$) earthquakes and be recorded by an OBS. The detecting threshold for the island station is a bit higher may due to the additional acoustic wave converted to elastic wave near the island.

We can predict the duration of the T-waves relatively well using the available 1000 m contour line in this region assuming Type 1 T-wave travel paths. Different paths correlate with different conversion points, and may represent different parts of the T-wave. But paths from multiple conversion points can arrive at the OBS at the same time.

It might be difficult to simulate the T-wave in Taiwan because there are so many paths from different conversion points on the 1000 m contour lines. In addition, elastic wave convert into acoustic waves at both sloping seafloor near the SOFAR-channel and abyssal seafloor also had been documented *Park et al.* [2001]. These imply that T-waves may have even more complicated travel paths.

Based on the synthetic waveform modeling using Type 1 path, we found that T-wave amplitude is correlated with the acceleration of the ground motions at the conversion points, which is the function of the earthquake radiation patterns and the travel path of the leg 1. The waveform amplitudes might decrease if there are gaps in the conversion points on the 1000 m contour lines. The synthetic waveforms were used to calculate the amplitudes of the T-wave at the different conversion points, most of the time, the S to T conversion generates larger T-wave amplitude than P to T conversion (Fig. 4). In terms of T-wave duration, we found that the Type 1 T-wave energy dominate the whole T-wave. However, sometimes we can not fit the amplitudes of the T-wave very well, especially



the later part of the T-wave, which might be related to the 3D crustal structures generating coda that can not be simulated using the 1D velocity model. There is also T-wave energy arriving earlier than our predicted Type 1 time window. We interpret that there might be contribution from Type 2 T-wave in the observed data.

For the abyssal earthquakes, we have also observed Type 2 T-waves. We have interpreted the energy to be T-wave, instead of the S wave coda from Type 3, because it is usually rare to have such long duration of S wave coda (~ 50 sec). In addition, the amplitude of the observed T-wave almost stays as big as the Type 3 S to T conversion. If it were Type 3 T-wave, the amplitude should decay as time increases like that in the ground motion. We have also compared the ratio of the seismic ground acceleration with the pressure changes, and found that at time “a”, there is a lower ratio, showing the energy is from the water column to the ground near the OBS. We interpret that this phase is the direct path from the abyssal earthquake to the SOFAR-channel, then going down to seafloor near the OBS site. In short, from traveltime and from two way transfer function analyses, we have evidence showing the T-wave can also be excited from the deep sea [e.g. *Yang and Forsyth*, 2003], and propagate into SOFAR-channel before being recorded at deep sea by the OBS.

Our traveltime analyses of the 60 events shed some light on using the different phases of the T-wave for relocation purpose. We think in some cases, it is better to pick the arrival time of the maximum amplitude T-wave, and use a great circle path to relocate the event using T-wave. However, such simple case can easily be complicated by energy from multiple conversion points that arrive at the same time, or by strong radiation pattern effects, or by the availability of the conversion points in the region. In addition, the arrival time of the maximum amplitudes of the filtered ground motions sometimes does not coincide with that of the DPG. Sometime such discrepancy can be up to tens of seconds.

The cause of such discrepancy is still unknown. In short, although it is better to use the arrival time of the maximum amplitude for relocation purpose, there are still many factors that need to be considered.

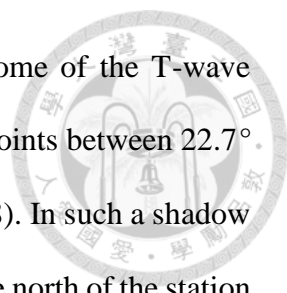


It is difficult to pick the first arrival of the T-wave because of its emergent feature. These early arrivals in our traveltime analyses have paths that follow the Snell's law and Fermat's law due to the large velocity contrast between elastic waves and the acoustic wave. Theoretically it is possible to use such early arrivals to help relocate the event. In reality, there is also some energy arriving before those "early arrival". We interpret that these energy to be Type 2 T-wave, which has shorten acoustic leg, and thus the earlier arrival time. In other words, there are multiple mechanisms that can generate the early arrivals of the T-wave, making it difficult for us to pick it for relocation purpose.

For Type 1 path, sometime it is possible to use the gap in the T-wave to help locate the events. In Taiwan region, the 1000 m contour line is not continuous. There are gaps of conversion points available to excite T-wave in some particular locations, and thus some particular arrival times. We have seen several examples of T-wave with reduced amplitudes in some short time windows that are correlated with these gaps in conversion points (e.g. Fig. 3, 5 & 8). Such observation led us to interpret the reduced strength of the T-wave to be due to the missing conversion points at 1000 m. It also helps us to be able to use the gap to help event relocation.

Multiple conversions in one path will also reduce the T-wave amplitude. The island station has lower detection threshold, maybe due to the additional conversion from water column to the crust near the station.

Sometimes the geometry of 1000 m contour line can also reduce the T-wave amplitude by blocking the direct path in SOFAR-channel from the conversion point to



the station. From our study using island stations, we found that some of the T-wave energy can be blocked by the 1000 m contour line. The conversion points between 22.7° N to 24° N do not have direct line of sight to the island station (Fig. 8). In such a shadow zone, conversion points produce T-wave that will first hit a cape to the north of the station before being recorded by the island station. Such paths will not generate strong T-wave. On the other hand, for the earthquakes further to the north, they can generate strong T-wave from the conversion points north of the shadow zone. We interpret this as the reason that we see more T-wave from earthquakes to the north than to the west for this island station.

Using the FK code we were able to generate synthetic ground motions at the 1000 m contour line, then simulate the amplitude envelope of the T-wave recorded by the OBS. The relatively good fits of the envelopes suggest that the T-wave amplitudes are affected by the earthquake radiation patterns. In other words, the T-wave waveforms contain information of the earthquake focal mechanism. It might be possible to extract earthquake focal mechanism using T-wave waveforms from one station by utilizing different ground motions at different conversion points along the 1000 m contour.

The ratio between ground accelerations and water pressure changes can be used as a tool to tell us whether the wave comes to the OBS from water column or from the crust. The two-way transfer function of incident energy from crust to the water should have a same ratio. But in Figures 10 and 11, it seems S wave incident has higher ratios than that of the P incident. However, we document that we can use this two-way transfer function to discriminate whether the T-wave energy comes from the water column or from crust.

Chapter 5 Conclusions



Previously, T-waves have been recorded and studied by land stations in Taiwan [Lin, 2001]. But this is the first time that T waves have been recorded by an OBS in this region. We found that all of the 60 $M_w > 3.3$ earthquakes in Taiwan region during July 2006 and September 2007 have generated T-waves on the OBS data. About 90% of the earthquakes also generated T-waves that were recorded by an island station. We have studied the duration of the T-waves from the 60 earthquakes using traveltime analyses by taking account of the conversion points along the 1000 m contour lines in this region. Based on these results, we have classified three different types of paths for the OBS energy to propagate from the earthquake to the OBS. We found the most efficient elastic to acoustic wave conversions occur on the seafloor with a water depth of 1000 m where the SOFAR-channel is located. The duration of the T-wave is consistent with the ray paths from the available conversion points in this region.

We have calculated synthetic waveforms at the 1000 m contour lines for different conversion points. The T-wave amplitude correlates with the sum of the P and S wave “acceleration” at the conversion points. This means that the radiation patterns of the earthquakes can also affect the T-wave amplitude at different time. Both P and S waves can be converted into T-waves, but in most cases S waves more effective to generate large amplitude T-waves. The T-wave amplitude depends on the particle motions that are normal to the slope of the seafloor.

Most of the time, if the earthquake is closer to the 1000 m contour lines, it is more accurate to use the arrival time of the highest amplitude of the T-wave to locate the earthquake using a great circle path with SOFAR-channel velocity.

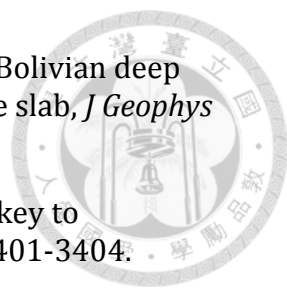
Although 1000 m contour lines provide effective conversion points, an abyssal earthquake can also transmit energy from deep sea to SOFAR-channel near the earthquake to generate T-wave, as seen in our abyssal earthquakes (Type 2). The T-wave then goes down to be recorded by an OBS at 4.7 km water depth.

Using the ratio between the ground accelerations and the acoustic pressure, we can estimate whether the energy arrives to the OBS from the ground or from the water column by analyzing the two-way transfer functions. We have used this to determine the paths of the early arrival energy for the abyssal earthquake to be from the water column. Because the two-way transfer functions are related to the elastic moduli of the crust and the water column, it might be possible to use such function to derive crustal property in the future.

Reference



- Aki, K., and P. G. Richards (1980), *Quantitative seismology : theory and methods*, W. H. Freeman, San Francisco.
- Balanche, A., C. Guennou, J. Goslin, and C. Mazoyer (2009), Generation of hydroacoustic signals by oceanic subseafloor earthquakes: a mechanical model, *Geophys J Int*, 177(2), 476-480.
- Butler, R. (2006), Observations of polarized seismoacoustic T waves at and beneath the seafloor in the abyssal Pacific ocean, *J. Acoust. Soc. Am.*, 120(6), 3599-3606.
- Cox, C., T. Deaton, and S. Webb (1984), A Deep-Sea Differential Pressure Gauge, *Journal of Atmospheric and Oceanic Technology*, 1(3), 237-246.
- Crawford, W. C., S. C. Webb, and J. A. Hildebrand (1991), Seafloor compliance observed by long-period pressure and displacement measurements, *Journal of Geophysical Research: Solid Earth*, 96(B10), 16151-16160.
- Crotwell, H. P., T. J. Owens, and J. Ritsema (1999), The TauP Toolkit: Flexible seismic travel-time and ray-path utilities, *Seismol Res Lett*, 70, 154-160.
- de Groot-Hedlin, C., and J. A. Orcutt (2001), Excitation of T-phases by seafloor scattering, *J Acoust Soc Am*, 109(5), 1944-1954.
- Fox, C. G., and R. P. Dziak (1998), Hydroacoustic detection of volcanic activity on the Gorda Ridge, February-March 1996, *Deep-Sea Res Pt Li*, 45(12), 2513-2530.
- Hanson, J., R. Le Bras, P. Dysart, D. Brumbaugh, A. Gault, and J. Guern (2001), Operational processing of hydroacoustics at the Prototype International Data Center, *Pure Appl Geophys*, 158(3), 425-456.
- Hanson, J. A., and J. R. Bowman (2006), Methods for monitoring hydroacoustic events using direct and reflected T waves in the Indian Ocean, *J Geophys Res-Sol Ea*, 111(B2).
- Kao, H., P. R. Jian, K. F. Ma, B. S. Huang, and C. C. Liu (1998), Moment-tensor inversion for offshore earthquakes east of Taiwan and their implications to regional collision, *Geophys Res Lett*, 25(19), 3619-3622.
- Lin, C. H. (2001), T-waves excited by S-waves and oscillated within the ocean above the southeastern Taiwan forearc, *Geophys Res Lett*, 28(17), 3297-3300.
- Linehan, D. (1940), Earthquakes in the West Indian Region, *Eos T Am Geophys Un*, 21, 229-232.
- Okal, E. A. (2008), The generation of T waves by earthquakes, *Advances in Geophysics*, 49, 1-65.

- 
- Okal, E. A., and J. Talandier (1997), T waves from the great 1994 Bolivian deep earthquake in relation to channeling of S wave energy up the slab, *J Geophys Res-Sol Ea*, 102(B12), 27421-27437.
- Park, M., R. I. Odom, and D. J. Soukup (2001), Modal scattering: a key to understanding oceanic T-waves, *Geophys Res Lett*, 28(17), 3401-3404.
- Rau, R. J., and F. T. Wu (1995), Tomographic Imaging of Lithospheric Structures under Taiwan, *Earth Planet Sc Lett*, 133(3-4), 517-532.
- Shin, T. C., and T. L. Teng (2001), An overview of the 1999 Chi-Chi, Taiwan, earthquake, *B Seismol Soc Am*, 91(5), 895-913.
- Shurbet, D. H. (1954), Bermuda T-Phases with Large Continental Paths, *Geol Soc Am Bull*, 65(12), 1350-1350.
- Shurbet, D. H., and M. Ewing (1957), T phases at Bermuda and transformation of elastic waves, *B Seismol Soc Am*, 47(3), 251-262.
- Slack, P. D., C. G. Fox, and R. P. Dziak (1999), P wave detection thresholds, Pn velocity estimates, and T wave location uncertainty from oceanic hydrophones, *J Geophys Res-Sol Ea*, 104(B6), 13061-13072.
- Thwaites, F. T., F. B. Wooding, J. D. Ware, Peal, K. R., and J. A. Collins (2005), A leveling system for an ocean-bottom seismometer, paper presented at IEEE Xplore.
- Yang, Y. J., and D. W. Forsyth (2003), Improving epicentral and magnitude estimation of earthquakes from T phases by considering the excitation function, *B Seismol Soc Am*, 93(5), 2106-2122.
- Zhu, L. P., and L. A. Rivera (2002), A note on the dynamic and static displacements from a point source in multilayered media, *Geophys J Int*, 148(3), 619-627.